Local measurement of vortex statistics in quantum turbulence

Eric Woillez[(a)], Jérôme Valentin and Philippe-E. Roche[(b)]

Univ. Grenoble Alpes, CNRS, Institut NEEL - F-38042 Grenoble, France

Abstract – The density fluctuations of quantum vortex lines are measured in a turbulent flow of superfluid He, at temperatures corresponding to superfluid fractions of 16%, 47% and 81%. The probe is a micro-fabricated second sound resonator allowing for local and small-scale measurements in the core of the flow, downstream a grid at a 10-mesh size. Remarkably, all the vortex power spectra collapse on a single master curve, independently from the superfluid fraction and the mean velocity. By contrast with previous measurements, we report a peculiar shape of the power spectra. The vortex density probability distributions are found to be strongly skewed, similarly to the vorticity distributions observed in classical turbulence. Implications of those results are discussed.

Introduction. – In the zero-temperature limit, quantum fluids behave at the macroscopic scale as a single coherent quantum state, the superfluid [1]. Compared to classical fluids, the quantum coherence of superfluids adds a strong constraint on the velocity field, namely to be irrotational. Rotational motion can only appear when the macroscopic coherence of the wave function is broken by topological defects called quantum vortices. In that case, the velocity circulation around the quantum vortex has a fixed value ($\kappa \simeq 10^{-7}\,\mathrm{m^2 s^{-1}}$ in ^{4}He). Turbulence in superfluids can be thought of as an intricate process of distortion, reconnection and breaking of those topological singularities [2], but in such a way that the system seems to mimic the classical turbulence at large scales [3]. This has been particularly obvious in the velocity spectra probed with a variety of anemometers, in highly turbulent flows [4–7] or in the measurement of vortex bundles using parietal pressure probes [8]. In some sense, quantum turbulence is an irreducible model, or to say it in a different way, is a kind of "skeleton" for all types of turbulence.

At finite temperature, the quantum fluid is not a pure superfluid: it behaves as if it experienced friction with a background viscous fluid, called the "normal fluid". The relative mass density of the superfluid ρ_s/ρ (where ρ is the total mass density) decreases from one at $0\,\mathrm{K}$ to zero at the superfluid transition temperature ($T_\lambda \simeq 2.18\,\mathrm{K}$ in ^{4}He). The presence of a finite normal fluid fraction

allows for propagation of temperature waves —a property referred to as "second sound"— which opens the rare opportunity to directly probe the presence of the quantum vortices [9].

This is done in the present article, where the statistics of superfluid vortex lines density $\mathcal{L}$ are locally measured by "second sound tweezer" (see the description in the section "Probes"), over one and a half decade in the inertial scales, and over a wide range of ρ_s/ρ spanning from 0.16 to 0.81. Surprisingly, the result does not corroborate the widespread idea that the large scales of quantum turbulence reproduce those of classical turbulence: the measured spectra of $\mathcal{L}$ (see fig. 6) differ from classical-like enstrophy spectra [10,11]. Besides, it also differs from the only[1] previous direct measurement of $\mathcal{L}$ with second sound tweezers [18] at $\rho_s/\rho \simeq 0.84$.

The measurement of the vortex lines density provides one of the very few constraints for the disputed modeling of the small scales of quantum turbulence. Even after intense numerical [19,20] and theoretical [21–23] studies, the statistics of quantum vortices show that even the large scales of quantum flows can still be surprising.

Experimental setup. – The experimental setup has been described in details in a previous publication [7]. In this section, we only review the major modifications. The setup consists in a wind tunnel inside a cylindrical

---

[(a)]E-mail: eric.woillez@neel.cnrs.fr (corresponding author)
[(b)]E-mail: philippe-emmanuel.roche@neel.cnrs.fr

[1]Literature also reports experimental [12] and numerical [13–17] spectra of the vortex line density spatially integrated across the whole flow. Still, spectra of such "integral" quantities differ in nature from the spectra of local quantities, due to strong filtering effects of spatial fluctuations.
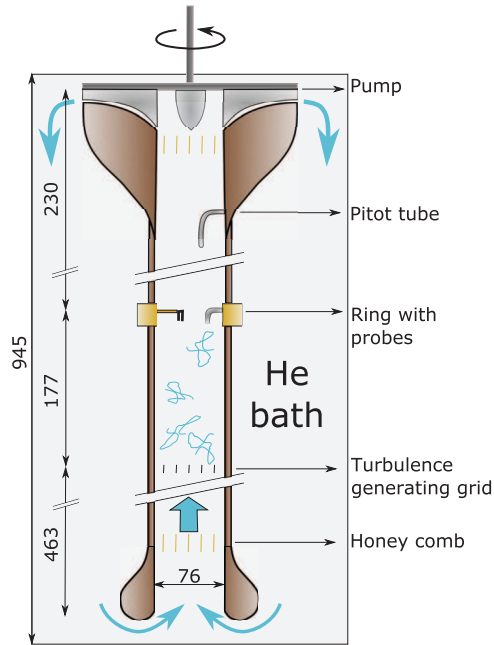
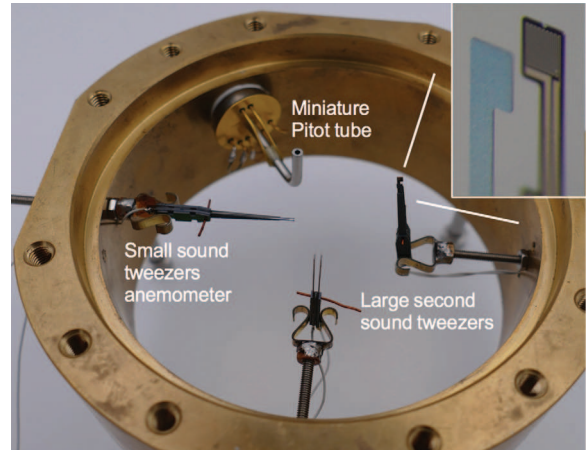Fig. 1: Sketch of the flow and the experimental setup with probes.

Fig. 2: Ring with probes. The inset is a zoom on the heating and thermometer plates of a second sound tweezers. The Pitot tube is not used in the present experiment.

cryostat (see fig. 1) filled with He-II. The flow is continuously powered by a centrifugal pump located at the top of the tunnel. At the bottom, an optimized 3D-printed conditioner ensures a smooth entry of the fluid, without boundary layer detachment, inside a $\Phi = 76$ mm inner diameter pipe. Spin motion is broken by radial screens built in the conditioner. The flow is then "cleaned" again by a 5-cm-long and 3-mm-cell honeycomb. The mean flow velocity U is measured with a Pitot tube located 130 mm upstream the pipe outlet. We allow a maximal mean velocity $U = 1.3$ m/s inside the pipe to avoid any cavitation effect with the pump.

The main new element compared to the previous design is a mono-planar grid located 177 mm upstream the probes, that generates turbulence. The grid has a $M = 17$ mm mesh with square bars of thickness $b = 4$ mm, which gives a porosity of $\beta = (1 - b/M)^2 \approx 0.58$.

The choice to position the probes at a distance $\sim 10M$ downstream the grid is the result of a compromise between the aim to have a "large" turbulence intensity, and the necessity to leave enough space for turbulence to develop between the grid and the probes. According to [24], this distance is long enough to avoid near-field effects of the grid. However, we emphasize that our main experimental results (figs. 6, 7) do not depend on perfect turbulent isotropy and homogeneity. *In situ* measurements of the mean vortex line density can be used to indirectly (via eq. (6)) give a turbulence intensity estimation $\tau = u^{\mathrm{rms}}/U \simeq 12$–13% (where u^{rms} is the standard deviation of longitudinal velocity component). We present the results later in fig. 5. For comparison, Vita *et al.* [24] report a turbulence intensity around $\tau = 9\%$ at $10M$ in a classical grid flow of similar porosity. The

difference between both τ values could originate from a prefactor uncertainty in eq. (6) or from differences in flow design (*e.g.*, the absence of a contraction behind the honeycomb). This difference has no important consequences for the measurement of quantum vortex statistics.

The longitudinal integral length scale of the flow $H \simeq 5.0$ mm is assessed by fitting velocity spectra (see bottom panel of fig. 6) with the von Kármán formula (*e.g.*, see [24]). For comparison, the integral scale reported for the similar grid in [24], once rescaled by the grid size, gives a nearby estimate of 7.4 mm.

The Reynolds number Re defined with $u^{\mathrm{rms}}H$ and the liquid He kinematic viscosity 1.8×10^{-8} m^{2}s^{-1} just above T_λ, is $Re = 3.3 \times 10^4$ for $U = 1$ m/s. Using the standard homogeneous isotropic turbulence formula, the Taylor scale Reynolds number is $R_\lambda = \sqrt{15Re} \approx 700$ (for $\tau = 12\%$ and $H = 5$ mm). This gives an indication of turbulence intensity below T_λ.

The helium bath temperature is set via pressure regulation gates. The He-II exceptional thermal conductivity ensures an homogeneous temperature inside the bath for $T < T_\lambda$. Two Cernox thermometers, one located just above the pump, the other one on the side of the pipe close to the probes, allow for direct temperature monitoring.

Probes. – Our probes are micro-fabricated second sound tweezers of millimeter size, according to the same principle as described in [18]. As displayed in the inset of fig. 2, the tweezers are composed of one heating plate and one thermometer plate facing each other and thus creating a resonant cavity for thermal waves. The heating plate generates a stationary thermal wave of the order of 0.1 mK between the plates, the amplitude of which can be recorded by the thermometer plate. Two major improvements have been done compared to the tweezers in [18]: first, the arms length supporting the plates has been increased to 14 mm to avoid blockage effects due to

the stack of silicon wafers (about 1.5 mm thick) downstream the cavity. Second, two notches are done in the arms to avoid interference due to additional reflections of the thermal wave on the arms. Further details will be given in a future publication.

In the presence of He flow, a variation of thermal wave amplitude and phase can be observed. This variation is due to two main physical effects. The presence of quantum vortex lines inside the cavity causes an attenuation of the wave [9,25] with a very minor phase shift [26]. This attenuation can be very accurately modeled by a bulk dissipation coefficient inside the cavity, denoted ξ_L. The second effect is a ballistic advection of the wave out of the cavity. It is related to both an attenuation of the temperature oscillation and to an important phase shift. Depending on the flow mean velocity U, the size of the tweezers, and the frequency of the wave, one of these two effects can overwhelm the other. We thus have designed two models of tweezers: one model to take advantage of the first effect to measure the vortex lines density (VLD), and the other one to take advantage of the second effect to measure the velocity.

The two largest tweezers displayed in fig. 2 are designed to measure the quantum vortex lines density. The plates size is $l = 1$ mm and the gaps between the plates are $D = 1.32$ mm and $D = 0.83$ mm, respectively. The plates face each other with a few micrometers positioning accuracy. The tweezers are oriented parallel to the flow (see fig. 2, the mean flow being directed from top to bottom) to minimize the effect of the wave ballistic advection.

The smallest tweezers displayed in fig. 2 are designed to be mainly sensitive to the velocity fluctuations parallel to the mean flow. The two plates have a size $l = 250\,\mu$m, and are separated by a gap $D = 0.431$ mm. The tweezers are oriented perpendicular to the mean flow (see fig. 2) with an intentional lateral shift of the heater and the thermometer of about $l/2$. This configuration is expected to maximize the sensitivity to ballistic advection, and thus to velocity fluctuations. To second order, however, the probe still keeps sensitivity to the quantum vortices produced both by turbulence and by the intense heating of the plates, that is why we were not able to calibrate it reliably. The (uncalibrated) spectrum of this probe (see bottom panel of fig. 6) is only used to estimate the integral length scale. The role of this probe is also to prove that the largest tweezers signal statistics are not due to velocity fluctuations.

Method. – Figure 3 displays a large tweezers resonance at frequency $f_0 = 15.2$ kHz, for increasing values of the mean velocity. The temperature oscillation T measured by the thermometer is demodulated by a lock-in amplifier NF LI5640. T can be accurately fitted by a classical Fabry-Perot formula

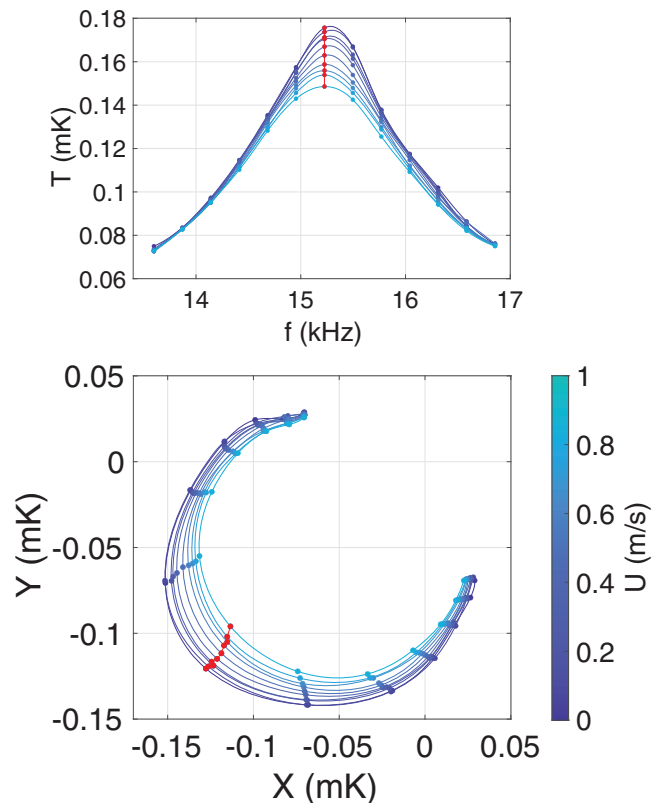$$T = \frac{A}{\sinh\left(i\frac{2\pi(f-f_0)D}{c_2} + \xi D\right)}, \tag{1}$$

Fig. 3: Top: second sound resonance of one of the large tweezers around 15.2 kHz. U increases from the top to the bottom curve. The vertical axis gives the thermal wave amplitude in K. Bottom: representation of the same resonance in phase and quadrature.

where $i^2 = -1$, f_0 is the resonant frequency for which the wave locally reaches its maximal amplitude, c_2 is the second sound velocity, A is a parameter to be fitted, and ξ is related to the wave energy loss in the cavity. The top panel of fig. 3 displays the amplitude of the thermal wave (in mK) as a function of the frequency, and the bottom panel shows the same signal in phase and quadrature. When the frequency is swept, the signal follows a curve close to a circle crossing the point of coordinates $(0,0)$. Figure 3 clearly shows that the resonant peak shrinks more and more when U increases, which is interpreted as wave attenuation inside the cavity. The red points display the signal attenuation at constant value of f. It can be seen on the bottom panel that the signal variation is close to a pure attenuation, that is, without phase shift. ξ can be decomposed as

$$\xi = \xi_0 + \xi_L, \tag{2}$$

where ξ_0 is the attenuation factor when $U = 0$ m/s and ξ_L is the additional attenuation created by the presence of quantum vortex lines inside the cavity. ξ_L is the interesting signal as it can be directly related to the vortex lines density (VLD) using the relations
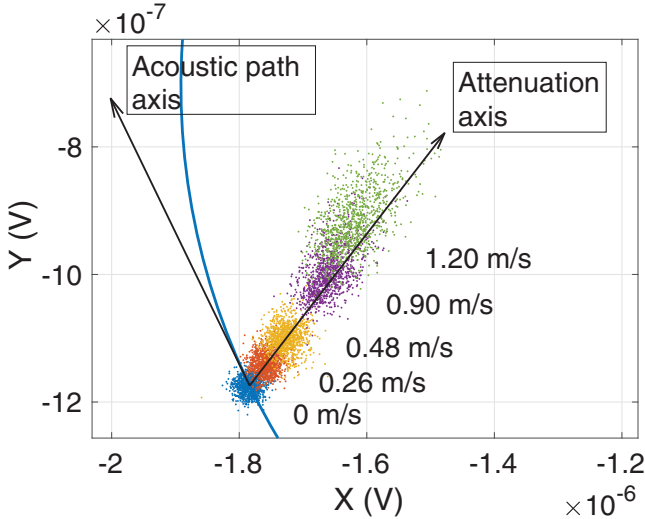
$$\xi_L = \frac{B\kappa L_\perp}{4c_2}, \tag{3}$$

Fig. 4: Fluctuations of the thermal wave in phase and quadrature. The colored clouds show the fluctuations of the signal, for different values of U. The blue curve shows the resonance for $U = 0\,\text{m/s}$. The fluctuations tangent to the resonant curve are created by a variation of the acoustic path. The quantum vortices are associated to attenuation of the wave and create a displacement along the attenuation axis.

$$L_\perp = \frac{1}{\mathcal{V}} \int \sin^2 \theta(l)\mathrm{d}l, \tag{4}$$

where B is the first Vinen coefficient, $\kappa \approx 9.98 \times 10^{-8}\,\text{m}^2/\text{s}$ is the quantum of circulation, $\mathcal{V}$ is the cavity volume, l is the curvilinear absciss along the vortex line, $\theta(l)$ is the angle between the vector tangent to the line and the direction perpendicular to the plates. We note that the summation is weighted by the distribution of the second sound nodes and antinodes inside the cavity and does not exactly correspond to a uniform average but we neglect this effect in the following. Our aim is to measure both the average value and the fluctuations of $L_\perp$, as a function of U and the superfluid fraction.

The method goes as follows: first, we choose a resonant frequency f_0 where the signal amplitude has a local maximum and we fix the heating frequency to this value f_0. Then we vary the mean velocity U and we record the thermometer plate response in phase and quadrature. The measurements show that the velocity-induced displacement in the complex plane follows a straight line in a direction $\vec{e}$ approximately orthogonal to the resonant curve. Expressions (1), (2) give ξ_L from the measured amplitude T by [18]

$$\xi_L = \frac{1}{D}\mathrm{asinh}\left(\frac{A}{T}\right) - \xi_0. \tag{5}$$

The colored dots of fig. 4 illustrate the signal fluctuations in phase and quadrature, for different values of U. The average signal moves in the direction of the attenuation axis. The figure also shows a part of the resonant
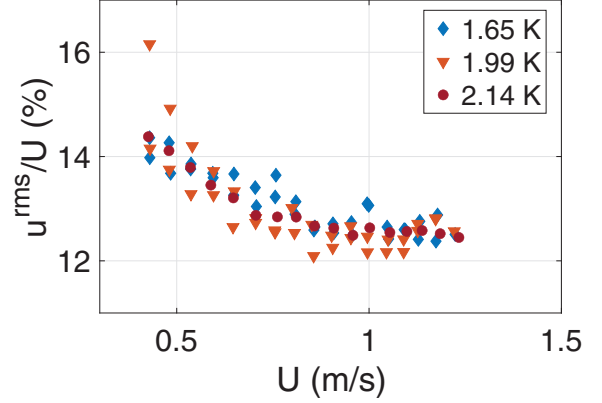

Fig. 5: Indirect measurement of the turbulence intensity $\tau = u^{\mathrm{rms}}/U$ as a function of U using eq. (6). The three different symbols correspond to three mean temperature values.

curve for $U = 0$. The fluctuations have two components in the plane, both associated with different physical phenomena. Fluctuations in the direction tangent to the resonant curve can be interpreted as a variation of the acoustic path $\frac{2\pi(f-f_0)D}{c_2}$ without wave attenuation. Those fluctuations can occur for example because the two arms of the tweezers vibrate with submicron amplitude, or because the temperature variations modify the second sound velocity c_2. To isolate only the fluctuations associated to attenuation by the quantum vortices, we split the signal into a component along the attenuation axis, and another one along the acoustic path axis. We then convert the displacement along the attenuation axis into vortex line density (VLD) using expressions (3)–(5).

Results. – As a check of the validity of our approach, we measured the average response of the second sound tweezers as a function of the mean velocity U. According to the literature [27], we were expecting the scaling $\langle L_\perp \rangle^2 \propto U^3$, with a prefactor related to the flow main characteristics. The function $\langle L_\perp \rangle$ was thus measured for a range $0.4 < U < 1.25\,\text{m/s}$ with a time averaging over 300 ms, at the three different temperatures $1.65\,\text{K}$, $1.99\,\text{K}$ and $2.14\,\text{K}$.

An effective superfluid viscosity ν_{eff} is customarily defined in quantum turbulence by $\epsilon = \nu_{\mathrm{eff}}(\kappa\mathcal{L})^2$ where ϵ is the dissipation and $\mathcal{L} = 3\langle L_\perp \rangle/2$ is the averaged VLD (we assume tangle isotropy) [28]. For large R_λ homogeneous isotropic flows, we also have $\epsilon \simeq 0.79\,U^3\tau^3/H$ (*e.g.*, see [29], p. 245), which entails

$$\tau^3 \simeq 2.85\frac{\nu_{\mathrm{eff}}H\kappa^2\langle L_\perp\rangle^2}{U^3}. \tag{6}$$

Using eq. (6), we compute the turbulence intensity as a function of U, for the three considered temperatures. The result is displayed in fig. 5. The figure shows that the turbulence intensity reaches a plateau of about 12% above $0.8\,\text{m/s}$, a value in accordance with the 9% turbulence intensity reported in [24], for a grid turbulence with similar
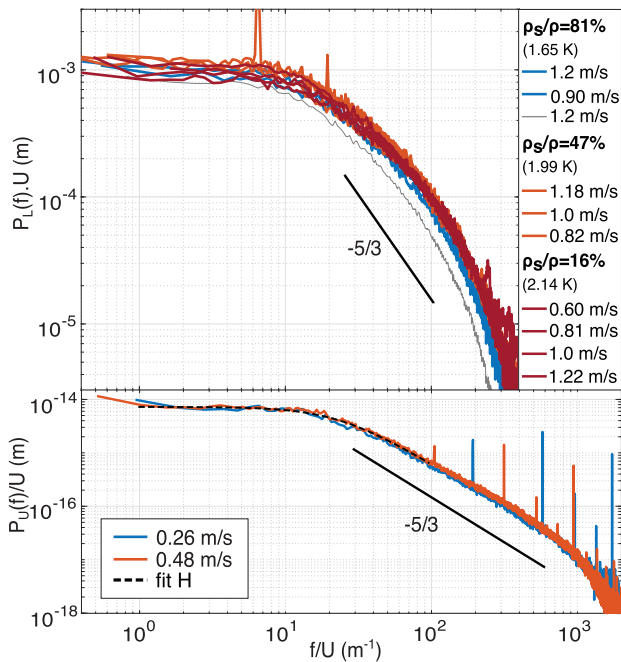
Fig. 6: Top: power spectral density of the projected vortex line density (VLD) $L_\perp$, obtained with the large second sound tweezers, for different values of U and temperatures. All measured spectra collapse using the scaling f/U and $P_L(f) \times U$. The fluctuations have been rescaled by the mean value of the VLD such that integrating the above curves directly gives the VLD turbulence intensity. Bottom: power spectral density of the uncalibrated velocity signal obtained from the second sound tweezers anemometer, for two values of U at 1.65 K. The spectra collapse using the scaling f/U for the frequency and $P_U(f)/U$ for the spectral density. The straight line displays the $-5/3$ slope which is expected for a classical velocity spectrum in the inertial range of the turbulent cascade. The dotted line is a fit using the von Kármán expression (see [24]) to find the integral scale H.

characteristics. The figure also confirms that the expected scaling $\langle L_\perp \rangle^2 \propto U^3$ is reached in our experiment for the velocity range $U > 0.8$ m/s.

The temperature-dependent viscosity ν_{eff} in eq. (6) has been measured in a number of experiments (*e.g.*, see in [23,27,30]). Still, the uncertainty on its value exceeds a factor 2. For the temperatures 1.65 K and 1.99 K, we used the average values 0.2κ and 0.25κ. By lack of reference experimental value of ν_{eff} above 2.1 K, we determined it by collapsing the $\tau(U)$ datasets obtained at 2.14 K with the other two. We found the value $\nu_{\text{eff}} \approx 0.5\kappa$ at 2.14 K.

Assuming isotropy of the vortex tangle, the value of $\mathcal{L}$ gives a direct order of magnitude of the inter-vortex spacing $\delta = 1/\sqrt{\mathcal{L}}$. We find $\delta \approx 5$ μm at 1.65 K and a mean velocity of 1 m/s. This shows the large scale separation between the inter-vortex spacing and the flow integral scale H, a confirmation of an intense turbulent regime.

Figure 6 presents the main result of this letter. On the top panel, we display the VLD power spectral density $P_L(f)$ of $L_\perp/\langle L_\perp \rangle$. With this definition, the VLD

turbulence intensity $L_\perp^{\text{rms}}/\langle L_\perp \rangle$ is directly given by the integral of $P_L(f)$. We measured the VLD fluctuations at the temperatures $T = 1.65$ K and superfluid fraction $\rho_S/\rho = 81\%$, $T = 1.99$ K and $\rho_S/\rho = 47\%$, $T = 2.14$ K and $\rho_S/\rho = 16\%$. At each temperature, the measurement was done for at least two different mean velocities.

The first striking result is the collapse of all the spectra independently of the temperature, when properly rescaled using f/U as coordinate (and $P_L(f) \times U$ as power spectral density to keep the integral constant). The VLD spectrum does not depend on the superfluid fraction even for vanishing superfluid fractions, when T comes very close to T_λ. Only one measurement with one of the large tweezers at $T = 1.650$ K gave a slight deviation from the VLD spectra master curve: it is displayed as the thin grey curve in fig. 6. We have no explanation for this deviation but we did not observe this particular spectrum either with the second tweezers or at any other temperature.

Second, the VLD spectrum has no characteristic power-law decay. We only observe that the spectrum follows an exponential decay approximately above $f/U > 100$ m^{-1}. This strongly contrasts with the velocity spectrum obtained with the small second sound tweezers anemometer (see bottom panel), which displays all the major features expected for a velocity spectrum in classical turbulence: it has a sharp transition from a plateau at large scale to a power law scaling close to $-5/3$ in the turbulent cascade inertial scales. Actually, it can be seen that the spectral decrease is less steep than $-5/3$, which can be due either to non-perfect isotropy and homogeneity, or more likely to the fact that the signal has some second-order corrections in addition to its dependence on velocity fluctuations. A fit of the transition using the von Kármán expression (see [24]) gives the value $H = 5$ mm for the longitudinal integral scale. As a side remark, the apparent cut-off above 10^3 m^{-1} is an instrumental frequency cut-off of the tweezers.

We find a VLD turbulent intensity close to 20%, which is significantly higher than the velocity turbulence intensity. We also checked that we obtain the same VLD spectrum using different resonant frequencies f_0.

Our measurements are limited by two characteristic frequencies. First, the tweezers average the VLD over a cube of side l, which means that our resolution cannot exceed $f/U > 1/l$. For the large tweezers, this sets a cut-off scale of 10^3 m^{-1}, much larger than the range of inertial scales presented in the top panel of fig. 6. Second, the resonator frequency bandwidth decreases when the second sound resonance quality factor increases. This again sets a cut-off scale given by $f/U = \xi_0 c_2/(2U)$. The worst configuration corresponds to the data obtained at 2.14 K and $U = 1.2$ m/s where the cut-off scale is about 600 m^{-1}. For this reason, the VLD spectra of fig. 6 are conservatively restricted to $f/U < 300$ m^{-1} which allows to resolve about one and a half decade of inertial scales.

Figure 7 displays some typical PDF of the rescaled VLD fluctuations $L_\perp/\langle L_\perp \rangle$ in semilogarithmic scale, for the
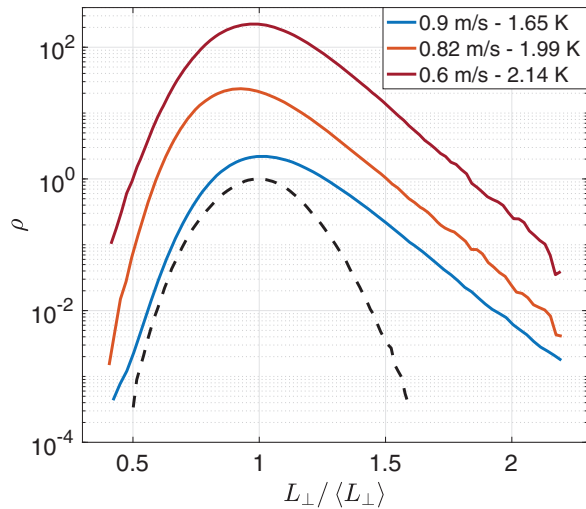
Fig. 7: Normalized probability distributions of the VLD fluctuations obtained at three temperatures. The PDF have been shifted by one decade from each other for readability. By comparison, the dotted black curve displays a rescaled PDF obtained with the small tweezers measuring velocity.

three considered temperatures. The PDF have been vertically shifted by one decade from each other for readability. The figure shows a strong asymmetry at all temperatures, with a nearly Gaussian left wing, and an exponential right wing. Contrarily to the VLD spectra, the PDF do not accurately collapse on a single master curve at different velocities and temperatures: yet, they remain very similar when the temperature and the mean velocity are changed, and their strongly asymetric shape seems to be a robust feature. By contrast, the dotted curve in fig. 7 displays one PDF of the small tweezers anemometer at 1.65 K, for which the mean has been shifted and the variance rescaled. It can be seen that the general shape of this latter PDF is much more symmetric and closer to a Gaussian as expected for a PDF of velocity fluctuations.

Discussion and conclusion. – In the present paper, we have investigated the temperature dependence of the vortex lines density (VLD) local statistics in quantum turbulence. About one and a half decade of turbulent cascade inertial scales was resolved. We measure the VLD mean value and deduce the turbulence intensity (fig. 5) from eq. (6). We report the VLD power spectrum (fig. 6), and the VLD probability distribution (fig. 7). Whereas the VLD mean value at different temperatures confirms previous numerical [19,27] and experimental studies [27], the spectral and PDF studies are completely new. Only one measurement of the VLD fluctuations had been done previously around 1.6 K [18] but in a wind tunnel with a very specific geometry and a non-controlled turbulence production. In the present work, we have used a grid turbulence, which is recognized as a reference flow with well-documented turbulence characteristics.

To conclude, we discuss below the three main findings:

1) A master curve of the VLD spectra, independent of temperature and mean velocity.

2) The observed master curve does not correspond to previously reported spectra in the context of highly turbulent classical flows.

3) A global invariant shape of the strongly skewed PDF.

The mean VLD gives the inter-vortex spacing, and thus tells how many quantum vortices are created in the flow, whereas the PDF and spectra tell how those vortices are organized in the flow. From 2.14 K to 1.65 K, our results confirm that the inter-vortex spacing only weakly decreases, by less than 23% for a 5-times increase of the superfluid fraction. In other words, the superfluid fraction has a limited effect on the creation of quantum vortices. The current understanding of the homogeneous isotropic turbulence in He-II is that the superfluid and normal fluid are locked together at large and intermediate scales where they undergo a classical Kolmogorov cascade [3]. The experimental evidences are based on the observation of classical velocity statistics using anemometers measuring the barycentric velocity of the normal and superfluid components. Here, the temperature independence of (normalized) VLD spectra supports this general picture, by reminiscence of a similar property of He-II velocity spectra.

In contrast to velocity, the observed VLD master curve has an unexpected shape in the inertial range, at odd with the spectra reported as "compatible with" a $f^{-5/3}$ scaling in [18]. The probe is sensitive to the total amount of vorticity in the scales smaller than the probe spatial resolution, and thus keeps track of the small scales fluctuations. A close classical counterpart of VLD is enstrophy, because its spectrum is also related to the velocity spectrum at smaller scales (*e.g.*, see [31]). However, the experimental [10] and numerical (*e.g.*, [11]) enstrophy spectra reported so far in three-dimensional classical turbulence strongly differ from the present VLD spectra. We have no definite explanation for this difference. It could originate from remanent quantum vortices pinned on the grid, that cause additional energy injection in the inertial range. In which case the peculiarity of our spectra would be specific to the type of forcing. Otherwise, it could be a more fundamental property associated with the microscopic structure of the vortex tangle that, together with the observed spectrum temperature independence, would be very constraining to develop mathematical closures for the continuous description of He-II (*e.g.*, see [32]).

As a discussion of the third statement, we compare the PDF with those of numerical simulations done in classical turbulence. The vorticity absolute value can be seen as a classical counterpart to the VLD. The work of Iyer

et al. [33], for example, displays some enstrophy PDF from high-resolution DNS, that can be compared to the PDF of fig. 7. At small scale, the enstrophy PDF are strongly asymmetric and will ultimately converge to a Gaussian distribution when averaged over larger and larger scales. Although our tweezers average the VLD over a size much larger than the inter-vortex spacing, they are small enough to sense short-life intense vortical events, typical of small scale phenomenology in classical turbulence. Thus, the strong asymmetry of the PDF supports the analogy between VLD and enstrophy (or its square root) and shows the relevance of VLD statistics to explore the small scales of quantum turbulence.

A side result of the present work is to obtain the relative values of the empirical coefficient $\nu_{\text{eff}} = \epsilon(\kappa\mathcal{L})^{-2}$ at the three considered temperatures. Models and simulations predict that ν_{eff} should steeply increase close to T_λ (see [23,27,30] and references therein), in apparent contradiction with the only systematic experimental exploration [34]. We found in fig. 5 that the effective viscosity ν_{eff} is twice larger at $2.14\,\text{K}$ than at $1.99\,\text{K}$. To the best of our knowledge, our estimate $\nu_{\text{eff}}(2.14\,\text{K}) \simeq 2\,(\pm 0.25) \times \nu_{\text{eff}}(1.99\,\text{K})$ is the first experimental hint of such an effective viscosity increase.

$$* * *$$

REFERENCES

[1] Donnelly R. J., *Quantized Vortices in Helium-II, Cambridge Studies in Low Temperature Physics* (Cambridge University Press, Cambridge) 1991.

[2] Barenghi C. F., Skrbek L. and Sreenivasan K. R., *Proc. Natl. Acad. Sci. U.S.A.*, **111** (2014) 4647.

[3] Barenghi C. F., L'vov V. S. and Roche P.-E., *Proc. Natl. Acad. Sci. U.S.A.*, **111** (2014) 4683.

[4] Maurer J. and Tabeling P., *Europhys. Lett.*, **43** (1998) 29.

[5] Salort J. *et al.*, *Phys. Fluids*, **22** (2010) 125102.

[6] Salort J., Chabaud B., Lévêque E. and Roche P.-E., *EPL*, **97** (2012) 34006.

[7] Rusaouen E., Chabaud B., Salort J. and Roche P.-E., *Phys. Fluids*, **29** (2017) 105108.

[8] Rusaouen E., Rousset B. and Roche P.-E., *EPL*, **118** (2017) 14005.

[9] Donnelly R. J., *Phys. Today*, **62,** issue No. 10 (2009) 34.

[10] Baudet C. and Hernandez R., *Spatial enstrophy spectrum in a fully turbulent jet*, in *Advances in Turbulence VI* (Springer) 1996, pp. 421–424.

[11] Ishihara T., Kaneda Y., Yokokawa M., Itakura K. and Uno A., *J. Phys. Soc. Jpn.*, **72** (2003) 983.

[12] Bradley D. I., Fisher S. N., Guénault A. M., Haley R. P., O'Sullivan S., Pickett G. R. and Tsepelin V., *Phys. Rev. Lett.*, **101** (2008) 065302.

[13] Fujiyama S. and Tsubota M., *J. Low Temp. Phys.*, **158** (2010) 428.

[14] Baggaley A. W. and Barenghi C. F., *Phys. Rev. B*, **84** (2011) 020504.

[15] Baggaley A. W., Laurie J. and Barenghi C. F., *Phys. Rev. Lett.*, **109** (2012) 205304.

[16] Baggaley A. W., Tsepelin V., Barenghi C. F., Fisher S. N., Pickett G. R., Sergeev Y. A. and Suramlishvili N., *Phys. Rev. Lett.*, **115** (2015) 015302.

[17] Tsepelin V., Baggaley A. W., Sergeev Y. A., Barenghi C. F., Fisher S. N., Pickett G. R., Jackson M. J. and Suramlishvili N., *Phys. Rev. B*, **96** (2017) 054510.

[18] Roche P.-E., Diribarne P., Didelot T., Français O., Rousseau L. and Willaime H., *EPL*, **77** (2007) 66002.

[19] Salort J., Roche P.-E. and Lévêque E., *EPL*, **94** (2011) 24001.

[20] Baggaley A. W., Barenghi C. F., Shukurov A. and Sergeev Y. A., *EPL*, **98** (2012) 26002.

[21] Roche P.-E. and Barenghi C. F., *EPL*, **81** (2008) 36002.

[22] Nemirovskii S. K., *Phys. Rev. B*, **86** (2012) 224505.

[23] Boué L., L'vov V. S., Nagar Y., Nazarenko S. V., Pomyalov A. and Procaccia I., *Phys. Rev. B*, **91** (2015) 144501.

[24] Vita G., Hemida H., Andrianne T. and Baniotopoulos C. C., *J. Wind Eng. Ind. Aerodyn.*, **178** (2018) 91.

[25] Varga E., Jackson M., Schmoranzer D. and Skrbek L., *J. Low Temp. Phys.*, **197** (2019) 130.

[26] Miller R., Lynall I. and Mehl J., *Phys. Rev. B*, **17** (1978) 1035.

[27] Babuin S., Varga E., Skrbek L., Lévêque E. and Roche P.-E., *EPL*, **106** (2014) 24006.

[28] Vinen W. F. and Niemela J. J., *J. Low Temp. Phys.*, **128** (2002) 167.

[29] Pope S., *Turbulent Flows* (Cambridge University Press) 2000.

[30] Gao J., Guo W., Yui S., Tsubota M. and Vinen W., *Phys. Rev. B*, **97** (2018) 184518.

[31] Antonia R., Shafi H. and Zhu Y., *Phys. Fluids*, **8** (1996) 2196.

[32] Nemirovskii S. K., *J. Low Temp. Phys.*, **201** (2020) 254.

[33] Iyer K. P., Schumacher J., Sreenivasan K. R. R. and Yeung P. K., *New J. Phys.*, **21** (2019) 033016.

[34] Stalp S., Niemela J. J., Vinen W. J. and Donnelly R. J., *Phys. Fluids*, **14** (2002) 1377.